Supporting information

Stretchable solvent-free ionic conductor with self-wrinkling microstructures for ultrasensitive strain sensor

Ying Ou, Tingting Zhao, Yang Zhang, Guanghui Zhao, Lijie Dong*

Center for smart materials and devices, state key laboratory of advanced technology for materials synthesis and processing, Wuhan University of Technology, Luoshi Road 122, Wuhan 430070, P.R. China

**Corresponding authors: Tel: (86) 27-87161730 Fax: (86) 27-87161730*

E-mail: dong@whut.edu.cn

This supporting file includes:

1. **Experimental Section**
2. **Supporting Tables**

Table S1 Composition ratio of as-prepared POSS-TMB-LiMTFSI

Table S2 Mechanical properties and crosslink density of as-prepared POSS-TMB-LiMTFSI

Table S3 Ionic conductivity of as-prepared POSS-TMB-LiMTFSI at different temperature

Table S4 Roughness and depth of wrinkled structure of as-prepared POSS-TMB-LiMTFSI

Table S5 Comparison of gauge factor at 100% tensile strain of this work with previously reported ionic resistive-type strain sensors

3. **Supporting Figures**

Fig. S1 (a) 1H NMR spectra of POSS-SH, LiMTFSI, and TMB, (b) 29Si NMR spectrum and TEM image of POSS-SH, (c) 11B NMR spectra of TMB and trimethyl borate

Fig. S2 (a, b) 1H NMR spectra of LiMTFSI monomer intermediate products

Fig. S3 (a) Transmittance in the visible range of 400–900 nm, (b) the weight change

of POSS-TMB-LiMTFSI at 20 °C and 60% relative humidity

Fig. S4 (a) E′ and E″ of POSS-TMB-LiMTFSI$_{0.33}$ with temperature sweep curve, (b) TGA curves of as-prepared POSS-TMB-LiMTFSI

Fig. S5 SEM images of as-prepared POSS-TMB-LiMTFSI

Fig. S6 EDS mappings of (a) B element, (b) F element, (c) S element, and (d) C element of POSS-TMB-LiMTFSI$_{0.33}$

Fig. S7 Survey XPS spectra of POSS-TMB-LiMTFSI ionic conductor with different Ar^+ sputtering time

Fig. S8 AFM images and surface analysis of (a) POSS-TMB-LiMTFSI$_0$, (b) POSS-TMB-LiMTFSI$_{0.11}$, (c) POSS-TMB-LiMTFSI$_{0.22}$, (d) POSS-TMB-LiMTFSI$_{0.33}$ and (e) POSS-TMB-LiMTFSI$_{0.44}$

Fig. S9 the relative resistance change rate under 100% strains

Fig. S10 Relationship between relative resistant change and temperature at 20% strain

Fig. S11 The relative resistance change rate at 20% strain under 0 - -20 °C

Fig. S12 Real-time tracking of human motion signals by the POSS-TMB-LiMTFSI strain sensor (a) wrist bending, (b) elbow bending, (c) knee bending, (d) ankle bending, (e) jumping and (f) sitting

Fig. S13 Real-time tracking of neck plus signals by the POSS-TMB-LiMTFSI strain sensor.

4. Supporting References

5. Supporting Video

Video S1 POSS-TMB-LiMTFSI ionic conductor adhered on various solid substrates

Video S2 POSS-TMB-LiMTFSI ionic conductor adhered and lifted the PTFE plate

Video S3 Relative resistance change of ionic conductor with the finger bending

1. Experimental Section

1.1 Materials:

(3-mercaptopropyl) triethoxysilane (95%), trimethyl borate (≥99.8%), poly(ethylene glycol) methacrylate (PEGMA, average M_n=360 g mol^{-1}), potassium 3-(methacryloyloxy)propane-1-sulfonate (98%), thionyl chloride (99%), dichloromethane (99.8%), trifluoromethanesulfonamide (95%), lithium hydride (95%), 1-hydroxycyclohexyl phenyl ketone (BP, 98%), tetrahydrofuran (THF), acetonitrile (CH_3CN, >99%), and dimethylformamide (DMF, 99.8%) were supplied from Aladdin (China). triethylamine (99.5%), hexane (97%), hydrochloric acid and methanol (AR) were obtained from Sinoparm chemical reagent Co. (China). THF and CH_3CN were dried with CaH_2 and distilled under reduced pressure before use. Lithium bis(trifluoromethanesulfonyl)imide (LiTFSI, 99%, , Aladdin, China) was stored in an argon-filled glovebox (H_2O_2 and O_2 contents ≤ 0.1 ppm)

1.2 Synthesis of thiol-functionalized POSS (POSS-SH)

(3-mercaptopropyl) triethoxysilane (10 g, 50.7 mmol) and methanol (200 mL) were added into a flask, and concentrated hydrochloric acid (20 mL) was then added under stirred. The reaction was performed in an oil bath at 90 °C for 24 hours. When the reaction completed, the solvent was removed, and the residue was dissolved in THF and precipitated in CH_3CN. Finally, the product (white crystal) was washed with methanol, then filtered, and dried at 80°C under vacuum for 24 h. ^{1}H NMR (400 M, $CDCl_3$): δ = 2.56 (2H, -C<u>H$_2$</u>-SH), 1.74 (2H, -C<u>H$_2$</u>-CH$_2$-SH), 1.39 (1H, -S<u>H</u>), 0.78 (2H,-Si-C<u>H$_2$</u>-) (Fig. S1a). ^{29}Si NMR: δ = -68 (s) (Fig. S1b). IR (KBr, cm^{-1}): 2545 cm^{-1} (-SH).

1.3 Synthesis of tris (2-methacryloyloxyethyl) borate (TMB)

Trimethyl borate (5.2 mL, 4.7 mmol) and PEGMA (5 g, 14mmol) were mixed in 50 mL anhydrous CH_3CN under N_2 atmosphere. The solution was stirred at 60 °C for 4 h, and the reaction temperature was then increased to 70 °C for another 3 h under N_2 purging to eliminate byproduct (CH_3OH). Residual solvent and unreacted trimethyl borate were removed by rotary evaporation at 50 °C. The obtained TMB was dried under vacuum at 25 °C over 48 h, and stored in an argon-filled glovebox (H_2O_2 and

O_2 contents ≤ 0.1 ppm). ^{1}H NMR (400 M, DMSO): δ =6.04 (1H, -(CH_3)C=C$\underline{H_2}$), 5.69(1H, -(CH_3)C=C$\underline{H_2}$), 4.21 (2H, -C$\underline{H_2}$-O-C(O)), 3.67-3.63 (H_2, -C$\underline{H_2}$-O-B), 3.57-3.45 (4H, -C$\underline{H_2}$-C$\underline{H_2}$-O), 1.89 (3H, -C$\underline{H_3}$) (Fig. S1a). ^{11}B NMR (400 M, $CDCl_3$) δ = 19.68 (Fig. S1c). IR (KBr, cm^{-1}): 1633cm^{-1} (C=C), 1294 cm^{-1} (B-O).

1.4 Synthesis of LiMTFSI

The LiMTFSI was synthesized based on a 3-step procedure according to the previous literature.

At first, potassium 3-(methacryloyloxy)propane-1-sulfonate (5.0 g) and DMF (catalyst, 0.57 mL) were added in anhydrous THF (8.5 mL) under N_2 atmosphere. Then, the reaction was cooled to 0 °C and thionyl chloride (13.3 g) was slowly added under stirring. After reacting at 0 °C for 1 h then at 25 °C for 12 h, the obtained suspension was drop-wise added into ice-water (67 mL). The oily layer was diluted with CH_2Cl_2 and washed with H_2O for 6 times, the solution was evaporated by rotary evaporation at 40 °C to remove CH_2Cl_2, and 3.7 g slightly yellow transparent oil was obtained. ^{1}H NMR (400 M, DMSO): δ =6.00 (1H, -(CH_3)C=C$\underline{H_2}$), 5.68(1H, -(CH_3)C=C$\underline{H_2}$), 4.16 (2H, -CH_2-O-C(O)), 3.67 (2H, –CH_2–SO_2Cl), 2.61 (2H, CO–O–CH_2–$\underline{CH_2}$–), 1.89 (3H, CH_2=C(CH_3)-) (Fig. S2a).

Secondly, the yellow transparent oil was diluted with anhydrous THF (5 mL), and then added into a mixed solution containing trifluoromethanesulfonamide (2.4 g), anhydrous trimethylamine (3.6 g) and anhydrous THF (13 mL) under N_2 atmosphere at 0 °C. After reacting at 0 °C for 1 h then at 25 °C for 2 h, the suspension was filtrated, and the filtrate was evaporated at 30 °C. Subsequently, the obtained yellow oily was diluted with CH_2Cl_2 and washed with H_2O for 4 times, the solution was evaporated by rotary evaporation at 40 °C to remove CH_2Cl_2. ^{1}H NMR (400 M, DMSO): δ =6.05 (1H, -(CH_3)C=C$\underline{H_2}$), 5.67(1H, -(CH_3)C=C$\underline{H_2}$), 4.19 (2H, -CH_2-O-C(O)), 3.14-3.04 (8H, H–N(C$\underline{H_2}$$CH_3$)$_3$ + –C$\underline{H_2}$–SO_2–N–), 2.07-1.97 (2H, O–CH_2–C$\underline{H_2}$–CH_2–), 1.87 (3H, CH_2=C(CH_3)-), 1.18 (9H, H–N(CH_2C$\underline{H_3}$)$_3$) (Fig. S2b).

Thirdly, the obtained yellow oily (3.3 g) was diluted with anhydrous THF (10 mL), and then LiH/THF suspension (0.09 g/15 mL) was slowly added at 0 °C under N_2 atmosphere. After that, the temperature was raised to 25 °C for 2 h. Then the obtained

suspension was filtrated to remove unreacted LiH, and the filtrate was washed with hexane for 3 times, the resulting LiMTFSI was evaporated under reduced pressure at 30 °C and stored in an argon-filled glovebox (H_2O_2 and O_2 contents ≤ 0.1 ppm). ^{1}H NMR (400 M, DMSO): δ =6.04 (1H, -(CH_3)C=C$\underline{H_2}$), 5.68(1H, -(CH_3)C=C$\underline{H_2}$), 4.19 (2H, -C$\underline{H_2}$-O-C(O)), 3.06 (2H, -C$\underline{H_2}$-SO_2−N);), 2.02 (2H, O–CH_2–C$\underline{H_2}$–CH_2–), 1.87 (3H, CH_2=C(CH_3)-), 1.87 (3H, CH_2=C(C$\underline{H_3}$)−) (Fig. S1a).

1.5 Fabrication of POSS-TMB-LiMTFSI solvent-free ionic conductor

The POSS-TMB-LiMTFSI solvent-free was fabricated by a UV-curing procedure. In the argon-filled glovebox (H_2O_2 and O_2 contents ≤ 0.1 ppm), predetermined weights of POSS-SH, TMB, LiMTFSI and photoinitiator BP (Table S1) dissolved in 0.75 M LiTFSI in THF. Then, the precursor solution were cast onto PTFE plate and exposed under a UV lighter (365 nm) for 30 min. The prepared membranes were dried in the argon-filled glovebox for 24 h.

1.6 Characterization

The Fourier transform infrared (FT-IR) spectra were recorded on a Thermo Nicolet AVATAR 360 (Thermo Co., USA) infrared spectrum analyzer. Nuclear magnetic resonance (NMR) spectra were performed on an AVANCE III HD (400 MHz, Bruker Co., Germany) at room temperature using d_6-DMSO and $CDCl_3$ as the solvent. The morphology of POSS-SH and POSS-TMB-LiMTFSI ionic conductor were observed by a transmission electron microscope (TEM, JEM-1400Plus, Hitachi Co., Japan) and field-emission scanning electron microscope (FESEM, JSM-5610LV, Hitachi Co., Japan). Atomic force microscopy (AFM, Nanoscope IV, VEECO Co, USA) was used to observe the surface morphology of ionic conductor. Uv-vis spectroscopy (UV, Lambde 750 S, PerkunElmer, USA) was used to measure the transmittance of ionic conductor. X ray photoelectron spectrometer (XPS, ESCALAB 250Xi, Thermo Fisher Scientific Co., USA) was conducted to investigate the surface chemical structure of ionic conductor with different depth, and the surface of POSS-TMB-LiMTFSI was etched by Ar^+ sputtering. The thermal stability of POSS-TMB-LiMTFSI ionic conductor was estimated by STA 499F (NETZSCH Co., Germany) thermogravimetric analyzer (TGA) from 100 °C to 800 °C under N_2. Dynamic thermomechanical

analysis (DMA) was performed from 25 to 80 °C at a heating rate of 3 °C min^{-1} with a fixed frequency of 1 Hz. Differential scanning calorimetry (DSC, DSC8500, PerkinElmer, USA) was performed to measure the glass transition temperatures (T_g) with a heating rate of 2 °C min^{-1} from -80 °C to 20 °C under N_2. The mechanical properties of the ionic conductor was investigated using a tensile testing machine (Instron 5967, Instron, USA) at a speed of 0.5 mm min^{-1} at room temperature. The simple was cut into 40 mm×10 mm specimens. The crosslink densities (v_e) of the POSS-TMB-LiMTFSI ionic conductors were measured by stress-strain method based on the basic rubber elasticity theory. The v_e can be determined from the initial modulus (Young's modulus E) with the following relationship $E=3v_eRT$.

1.7 Density Functional Theory (DFT) Study:

The simulation was performed by the DFT in Material Studio. According to Dmol3/GGA-PBE/DNP (3.5) basis set 1(3), the physical wave function was expanded.

The interaction energy (E_{int}) is calculated according to the following equation

$$E_{int} = E_{total} - E_{\text{components}}$$

Where E_{total} and $E_{components}$ represent the total energy of the system, and the energy of each component, respectively. And the E_{int} indicates the intensity of interaction between the components in the system.

1.8 Self-Healing Experiments

As-prepared ionic conductor (40 mm×10 mm) was cut into halves. Then get in touch with the two halves immediately at room temperature without applied stress and store them in a sealed container to isolate the interference of the external environment. After a certain self-healing time, the uniaxial tensile test was carried out to evaluate the healing efficiency (HE). The HE is defined as the ratio of fracture strength between the healed and the original sample.

1.9 Lap Shear Tests.

A tensile testing machine was used to investigate the adhesion performance of the ionic conductor by the lap shear tests. A POSS-TMB-LiMTFSI ionic conductor (10 mm × 10 mm × 0.3 mm) was placed between two substrates including glass, rubbers, Al, Cu, paper, PET and PTFE (50 mm × 10 mm) to form a sandwiched area of 10 mm

× 10 mm. Apply pressure of about 100 g for 10 min to form a good contact before the tests. The tensile tests were carried out at room temperature with a shear rate of 10 mm min^{-1}.

2.0 Electrochemical measurements

The ion conductivities of ionic conductor with the temperature range from 15 °C to 60 °C were measured by electrochemical impedance spectroscopy (EIS) on an electrochemical workstation (CHI660D, Chenhua Co., China) with the frequency range from 0.1 Hz to 10^6 Hz. The ionic conductor was sandwiched between two stainless steel (SS) block electrodes. The calculation formula of ionic conductivity (σ, S cm^{-1}) is as follows:

$$\sigma = \frac{L}{R \cdot A}$$

Where *L* (cm), *R (Ω)* and *A* (cm^{-2}) represent the thickness of the ionic conductor, bulk resistance, and the contact area between the ionic conductor and SS, respectively.

2.1 Preparation and Test of resistive-type strain sensors

The POSS-TMB-LiMTFSI ionic conductor with a size of 20 mm × 10 mm × 0.3 mm was used as the core component of the resistive-type strain sensor. Two Cu foil with a width of 10 mm was used as electrodes at both ends. In addition, an additional two layers of VHB films were put on the top and bottom of the sensor to insulate the sensor, thus eliminating interference from gas and humidity. The resistance change of ionic conductor in accordance with applied strains were recorded on a desktop multimeter (7510, Keithley, USA). The gauge factor is defined as $GF=d(\Delta R/R_0)/d\varepsilon$, where the $\Delta R/R_0$ is relative resistance change rate of the ionic conductor under strain, and ε is the strain of the ionic conductor. Moreover, the strain sensor was placed on a heating table. The influence of temperature on its resistance change under 20% strain was recorded. To investigate the feasibility for wearable strain sensor, the POSS-TMB-LiMTFSI ionic conductor based strain sensor was fixed onto body joints of a volunteer under informed consent to sense the motion.

2. Supporting Tables

Table S1 Composition ratio of as-prepared POSS-TMB-LiMTFSI

Sample	POSS-SH (mmol)	LiMTFSI (mmol)	TMB (mmol)	BP (wt.%)
POSS-TMB-LiMTFSI$_0$	0.01	0	0.08	5
POSS-TMB-LiMTFSI$_{0.11}$	0.01	0.01	0.07	5
POSS-TMB-LiMTFSI$_{0.22}$	0.01	0.02	0.06	5
POSS-TMB-LiMTFSI$_{0.33}$	0.01	0.03	0.05	5
POSS-TMB-LiMTFSI$_{0.44}$	0.01	0.04	0.04	5

Table S2 Mechanical properties and crosslink density of as-prepared POSS-TMB-LiMTFSI

Sample	Young's modulus (MPa)	Elongation at break (%)	Tensile strength (MPa)	Crosslink density v_e (mol/m^3)
POSS-TMB-LiMTFSI$_0$	1.07	88.96	0.37	49.78
POSS-TMB-LiMTFSI$_{0.11}$	0.95	98.61	0.34	45.74
POSS-TMB-LiMTFSI$_{0.22}$	0.82	104.91	0.31	41.71
POSS-TMB-LiMTFSI$_{0.33}$	0.52	116.23	0.26	34.98
POSS-TMB-LiMTFSI$_{0.44}$	0.51	98.24	0.21	28.25

Table S3 Ionic conductivity of as-prepared POSS-TMB-LiMTFSI at different temperature

Sample	σ 15 °C (mS cm^{-1})	σ 30 °C (mS cm^{-1})	σ 40 °C (mS cm^{-1})	σ 50 °C (mS cm^{-1})	σ 60 °C (mS cm^{-1})	E_a (kJ mol^{-1})
POSS-TMB-LiMTFSI$_0$	0.19 (±0.053)	0.39 (±0.028)	0.68 (±0.101)	1.09 (±0.063)	1.63 (±0.407)	17.03
POSS-TMB-LiMTFSI$_{0.11}$	0.31 (±0.030)	0.67 (±0.037)	1.05 (±0.087)	1.75 (±0.135)	2.54 (±0.329)	16.63
POSS-TMB-LiMTFSI$_{0.22}$	0.52 (±0.031)	1.01 (±0.086)	1.56 (±0.124)	2.34 (±0.132)	3.52 (±0.294)	14.77
POSS-TMB-LiMTFSI$_{0.33}$	1.17 (±0.056)	1.73 (±0.103)	2.58 (±0.212)	4.23 (±0.251)	5.93 (±0.413)	12.80
POSS-TMB-LiMTFSI$_{0.44}$	2.30 (+0.041)	2.85 (±0.113)	4.62 (±0.381)	5.81 (±0.286)	9.04 (±0.399)	11.53

Table S4 Roughness and depth of wrinkled structure of as-prepared POSS-TMB-LiMTFSI

Sample	Roughness (nm)	Depth (nm)
POSS-TMB-LiMTFSI$_0$	38.73 (±6.21)	126.94 (±11.27)
POSS-TMB-LiMTFSI$_{0.11}$	48.48 (±5.36)	179.88 (±6.56)
POSS-TMB-LiMTFSI$_{0.22}$	63.05 (±6.81)	214.44 (±14.50)
POSS-TMB-LiMTFSI$_{0.33}$	86.71 (±5.17)	238.62 (±16.06)
POSS-TMB-LiMTFSI$_{0.44}$	92.65 (±7.03)	247 (±16.47)

Table S5 Comparison of gauge factor at 100% tensile strain of this work with previously reported

ionic resistive-type strain sensors

Sample	Gauge Factor at 100% tensile strain	Ref.
POSS-TMB-LiMTFSI	7.03	This work
LA-based ionic conductor	2.30	[1]
88-PMMA-r-PBA ion gel	2.73	[2]
TA@HAP NWs-PVA hydrogel	2.84	[3]
PAAm/PAA–Fe^{3+}/NaCl hydrogels	1.23	[4]
[C_2mim][NTf_2]-based ionic conductor	1.83	[5]
STP hydrogel	2.0	[6]
SBMS/HEMA/clay	1.8	[7]
P(MEA-co-IBA)	4	[8]

3. Supporting Figures

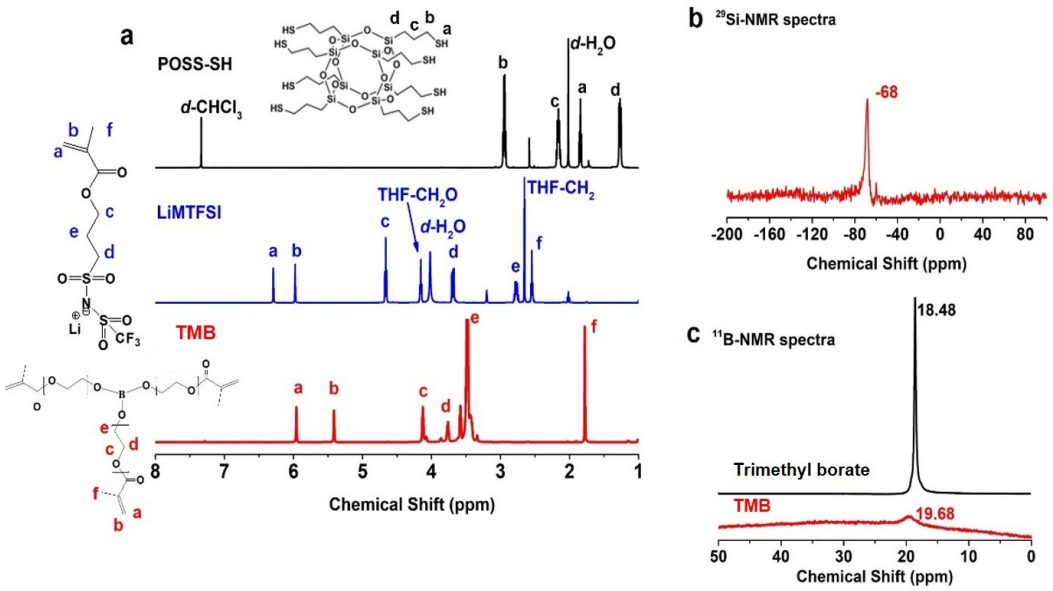

Fig. S1 (a) ^{1}H NMR spectra of POSS-SH, LiMTFSI, and TMB, (b) ^{29}Si NMR spectrum and TEM image of POSS-SH, (c) ^{11}B NMR spectra of TMB and Trimethyl borate

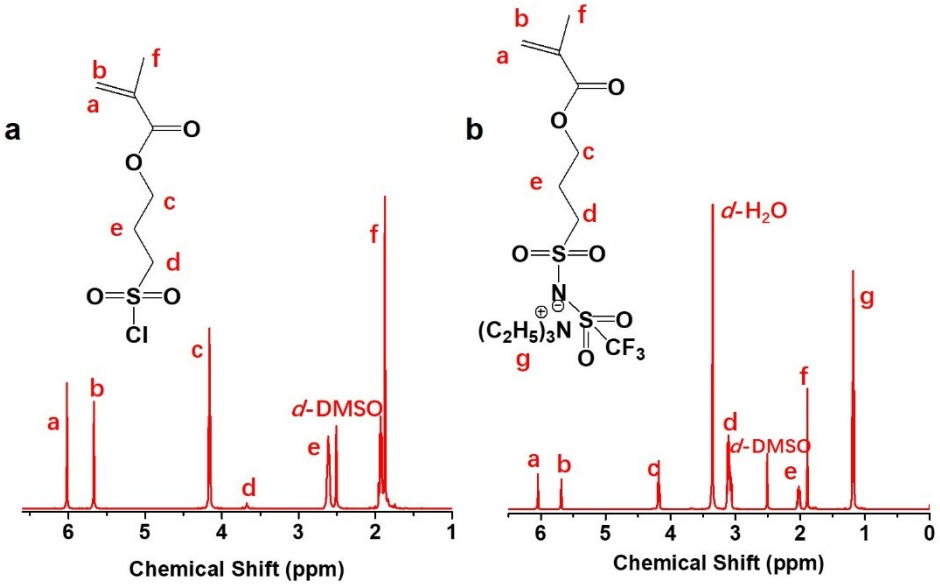

Fig. S2 (a, b) ^{1}H NMR spectra of LiMTFSI monomer intermediate products

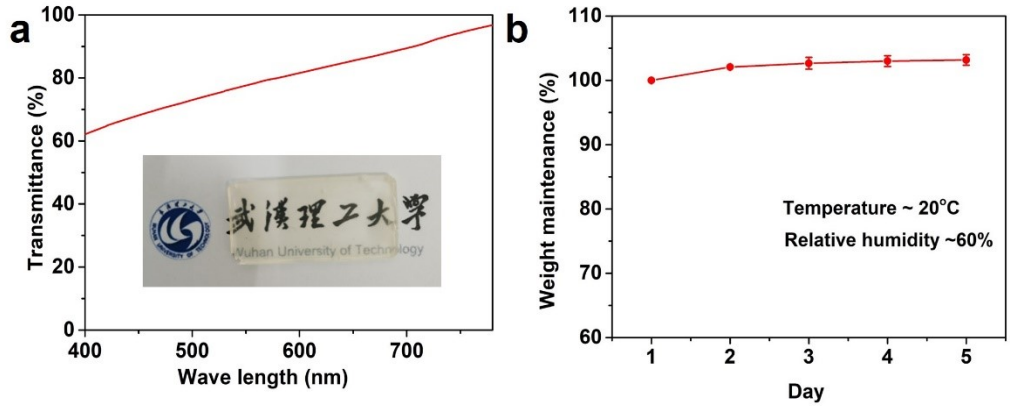

Fig. S3 (a) Transmittance in the visible range of 400–900 nm, (b) the weight change of POSS-TMB-LiMTFSI at 20 °C and 60% relative humidity

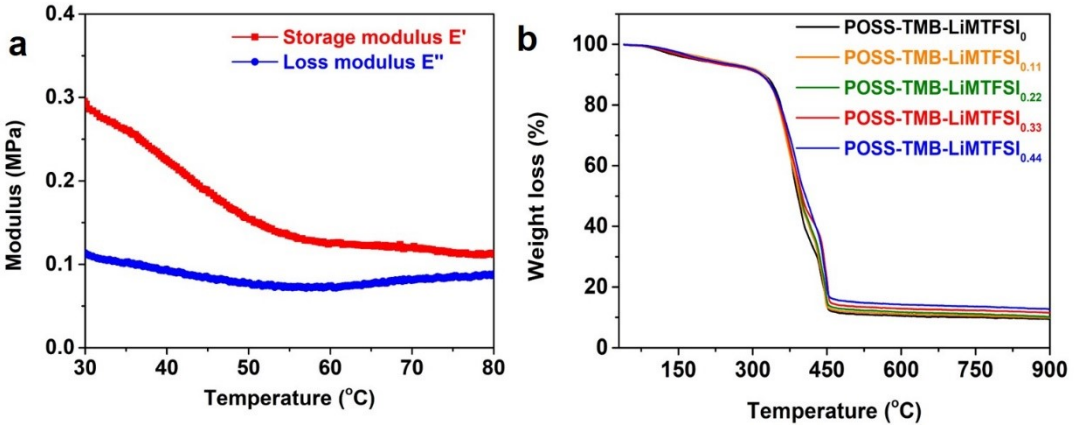

Fig. S4 (a) E′ and E″ of POSS-TMB-LiMTFSI$_{0.33}$ with temperature sweep curve, (b) TGA curves of as-prepared POSS-TMB-LiMTFSI

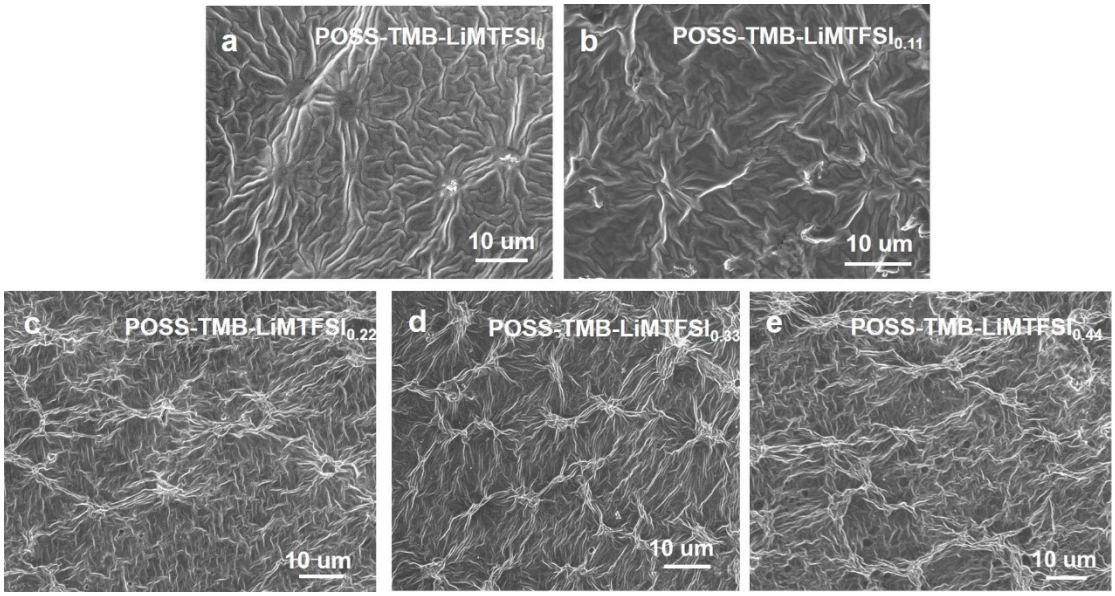

Fig. S5 SEM images of as-prepared POSS-TMB-LiMTFSI

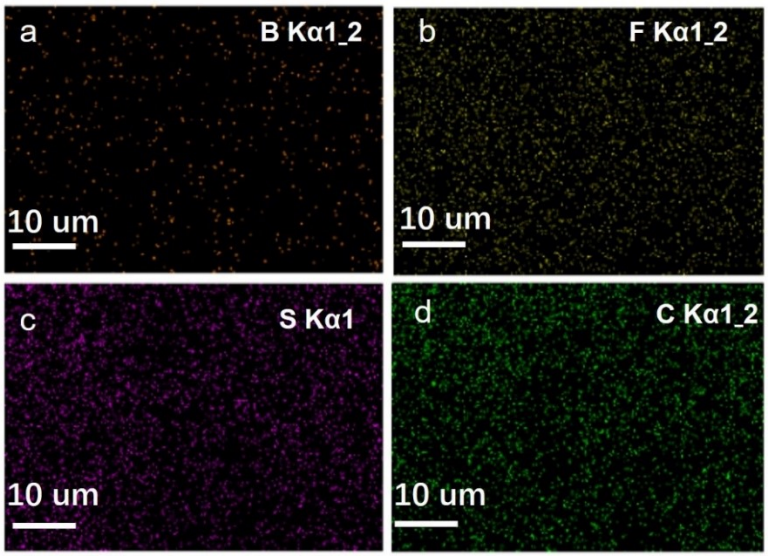

Fig. S6 EDS mappings of (a) B element, (b) F element, (c) S element, and (d) C element of POSS-TMB-LiMTFSI$_{0.33}$

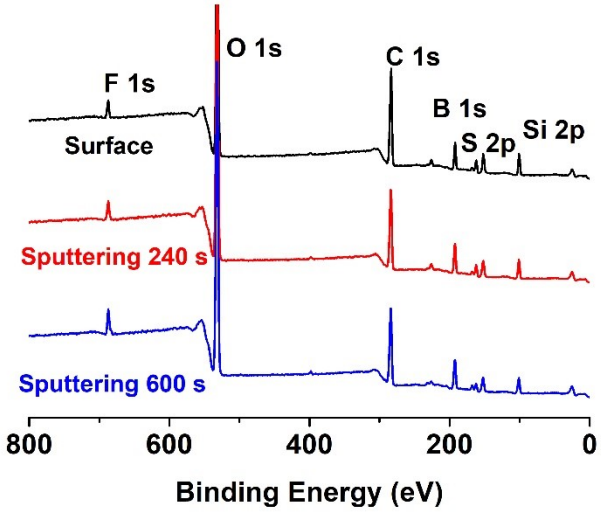

Fig. S7 Survey XPS spectra of POSS-TMB-LiMTFSI$_{0.33}$ ionic conductor with different Ar^+ sputtering time

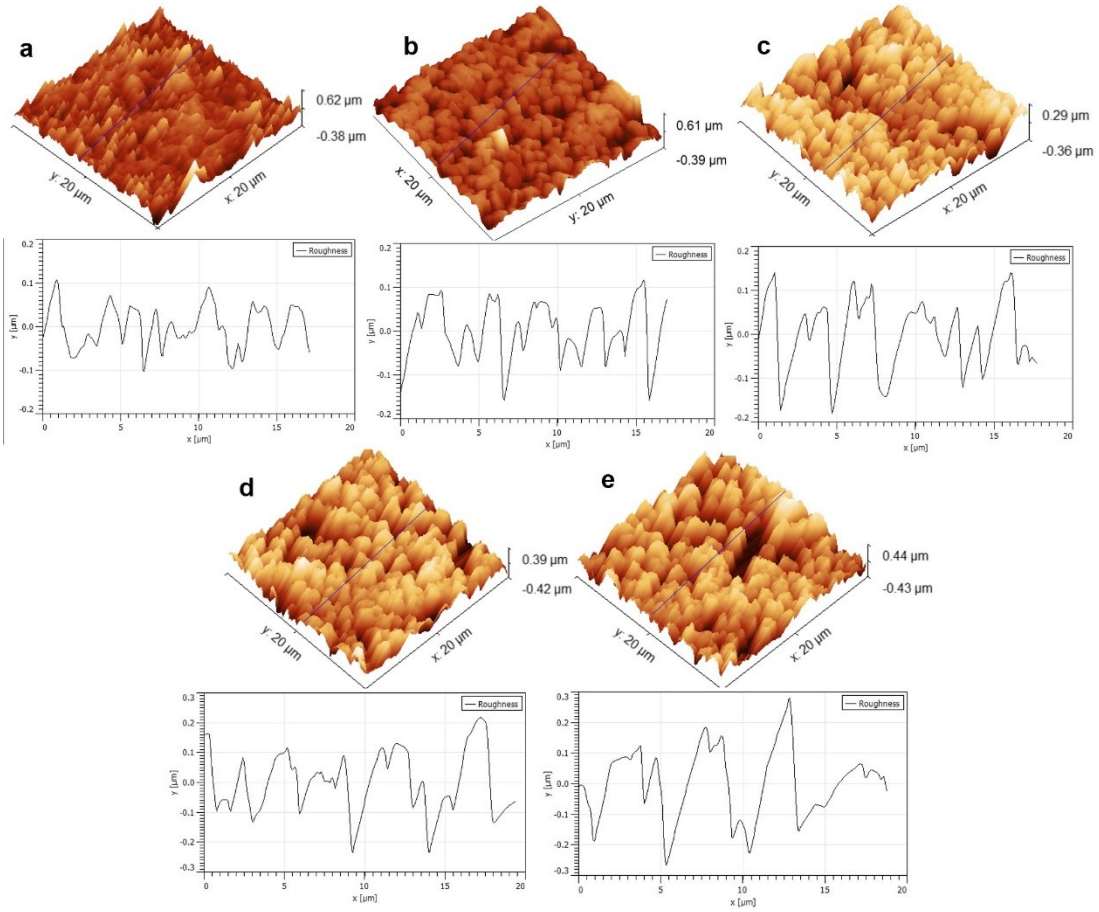

Fig. S8 AFM images and surface analysis of (a) POSS-TMB-LiMTFSI$_0$, (b) POSS-TMB-LiMTFSI$_{0.11}$, (c) POSS-TMB-LiMTFSI$_{0.22}$, (d) POSS-TMB-LiMTFSI$_{0.33}$ and (e) POSS-TMB-LiMTFSI$_{0.44}$

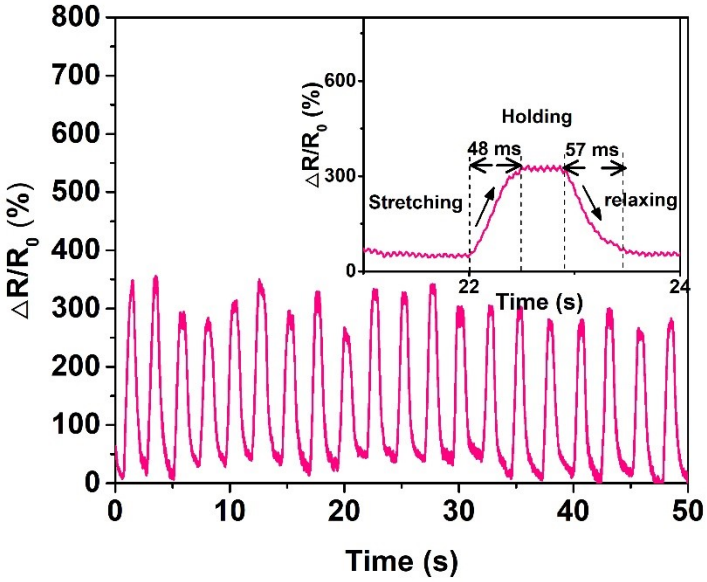

Fig. S9 The relative resistance change rate under 100% strains

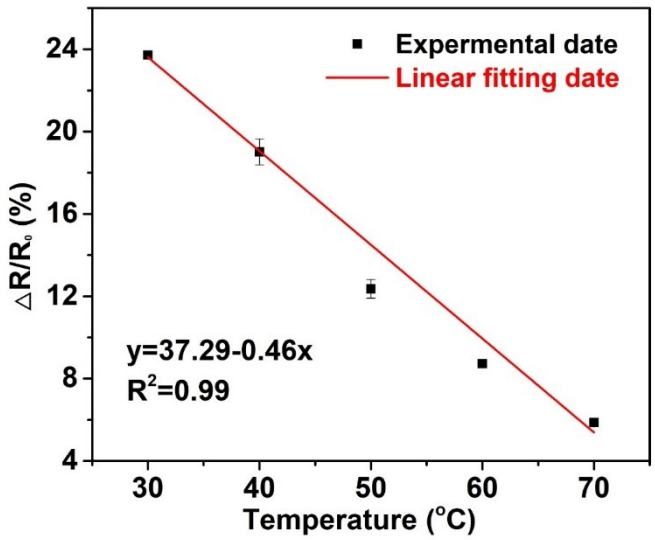

Fig. S10 Relationship between relative resistant change and temperature at 20% strain

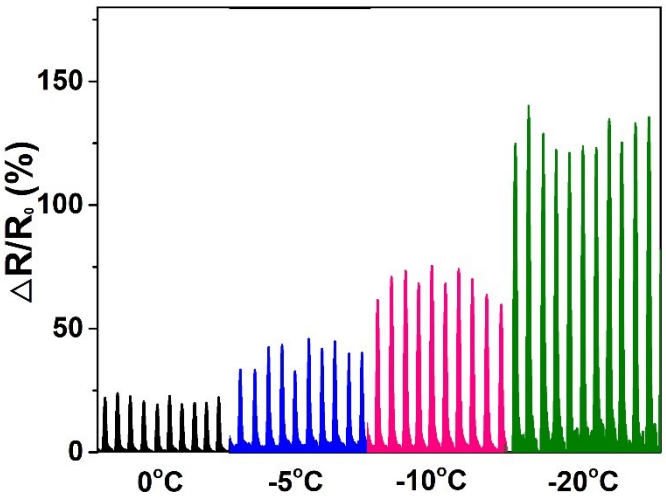

Fig. S11 The relative resistance change rate at 20% strain under temperature range of 0 - -20 °C

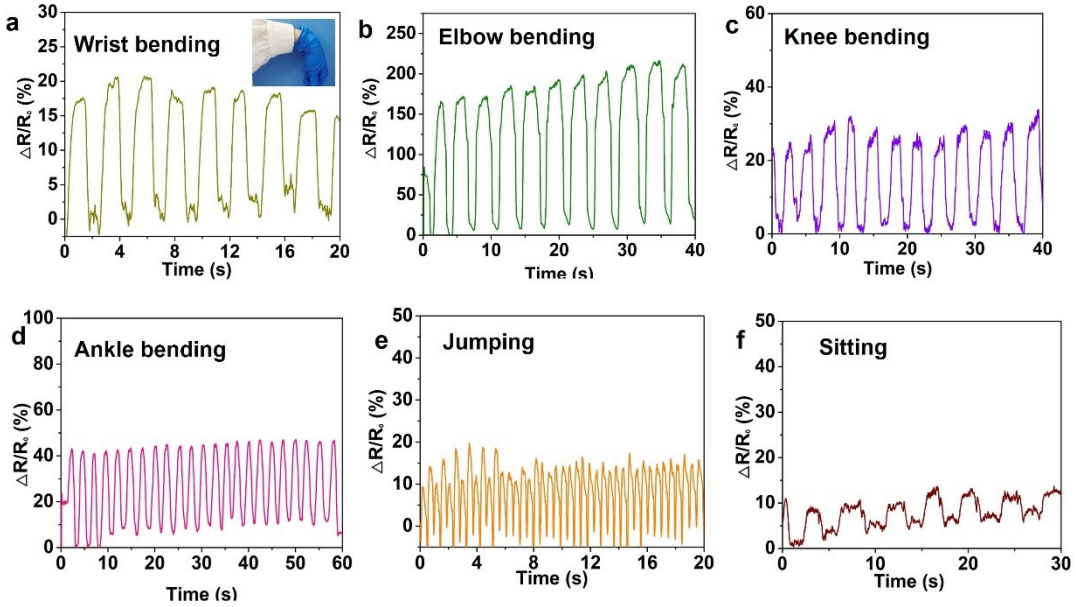

Fig. S12 Real-time tracking of human motion signals by the POSS-TMB-LiMTFSI strain sensor. (a) wrist bending, (b) elbow bending, (c) knee bending, (d) ankle bending, (e) jumping, and (f) sitting.

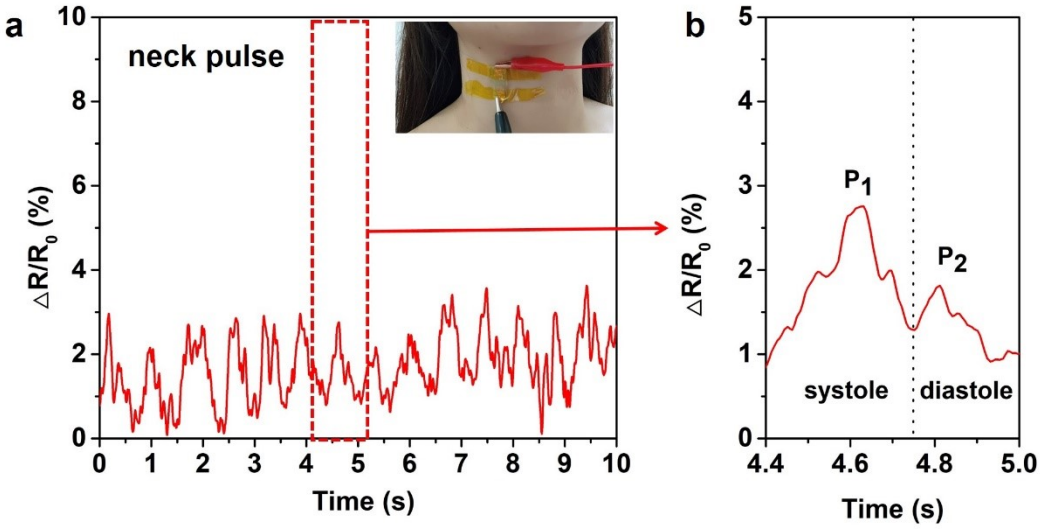

Fig. S13 Real-time tracking of neck plus signals by the POSS-TMB-LiMTFSI strain sensor

References

1. C. Dang, M. Wang, J. Yu, Y. Chen, S. Zhou, X. Feng, D. Liu and H. Qi, *Adv. Funct. Mater.*, 2019, **29**, 1902467.
2. Y. M. Kim and H. C. Moon, *Adv. Funct. Mater.,* 2019, **30**, 1907290.
3. J. Wen, J. Tang, H. Ning, N. Hu, Y. Zhu, Y. Gong, C. Xu, Q. Zhao, X. Jiang, X. Hu, L. Lei, D. Wu and T. Huang, *Adv. Funct. Mater.,* 2021, DOI: 10.1002/adfm.202011176, 2011176.
4. S. Li, H. Pan, Y. Wang and J. Sun, *J. Mater. Chem. A*, 2020, **8**, 3667-3675.
5. Z. Cao, H. Liu and L. Jiang, *Mater. Horiz.,* 2020, **7**, 912-918.
6. H. Qiao, P. Qi, X. Zhang, L. Wang, Y. Tan, Z. Luan, Y. Xia, Y. Li and K. Sui, *ACS Appl. Mater. Inter.*, 2019, **11**, 7755-7763.
7. L. Wang, G. Gao, Y. Zhou, T. Xu, J. Chen, R. Wang, R. Zhang and J. Fu, *ACS Appl. Mater. Inter.*, 2019, **11**, 3506-3515.
8. B. Yiming, Y. Han, Z. Han, X. Zhang, Y. Li, W. Lian, M. Zhang, J. Yin, T. Sun, Z. Wu, T. Li, J. Fu, Z. Jia and S. Qu, *Adv. Mater.*, 2021, **33**, e2006111.